Spin observables for the ^{208}Pb$(p,n)^{208}$Bi reaction at 135 MeV

Marco R. Plumley,[1] J. W. Watson,[1] B. D. Anderson,[1] A. R. Baldwin,[1] C. C. Foster,[2] R. Madey,[1] P. J. Pella,[3] E. Ramström,[4] W. Unkelbach,[5] and Y. Wang[1,2]

[1]*Department of Physics, Kent State University, Kent, Ohio 44242*

[2]*Indiana University Cyclotron Facility, Bloomington, Indiana 47405*

[3]*Department of Physics, Gettysburg College, Gettysburg, Pennsylvania 17325*

[4]*Uppsala University, Uppsala, Sweden*

[5]*Indiana University Nuclear Theory Center, Bloomington, Indiana 47405*

(Received 5 March 1996; revised manuscript received 21 February 1997)

We measured the spin observables A_y, P, and $S_{NN'}$ for the ^{208}Pb$(p,n)^{208}$Bi reaction at 135 MeV at laboratory angles of 0°, 3°, 6°, and 9°. The overall energy resolution was about 1 MeV. Data for $S_{NN'}$ are compared with distorted-wave impulse-approximation calculations that use random-phase approximation wave functions. Comparisons are also made for the ^{48}Ca$(p,n)^{48}$Sc reaction. The agreement between these calculations and the data is generally good, after adjustment of the nucleon-nucleon interaction in the random-phase approximation calculations to place the 0^+ isobaric-analog states at the correct excitation energies. A single adjustment of the nucleon-nucleon force works for both target nuclei. [S0556-2813(97)03107-5]

PACS number(s): 24.70.+s, 25.40.−h, 25.40.Kv

I. INTRODUCTION

The study of the nuclear spin-isospin response with medium energy probes has been an area of intense interest for nuclear physics. Particularly useful in these studies have been nucleon charge-exchange reactions because they are purely isovector. The measurement of spin observables has also proved quite useful in probing the nuclear spin response. Over the past several years we have undertaken a series of studies of spin observables for the (p,n) reaction on the doubly magic targets ^{16}O, ^{40}Ca, ^{48}Ca, and ^{208}Pb at 135 MeV. The observables we measured were the analyzing power $A_y(\theta)$, the induced polarization $P(\theta)$, and the transverse polarization transfer coefficient $D_{NN'}(\theta)$; for the scattering of spin 1/2 particles polarized normal to the reaction plane only these spin observables are measurable. The general relationship between these three observables, the polarization of the incident particle ($\equiv p_p$), and the polarization of the scattered particle ($\equiv p_n$) is

$$p_n[1+p_pA_y(\theta)]=P(\theta)+p_pD_{NN'}(\theta). \tag{1}$$

The spin-flip probability $S_{NN'}$ is related to $D_{NN'}$:

$$S_{NN'}=(1+D_{NN'}/2). \tag{2}$$

Our spin-observable studies of the (p,n) reaction on ^{16}O, ^{40}Ca, ^{48}Ca, and ^{208}Pb were made with a high-efficiency neutron polarimeter described in Ref. [1]. We reported the data for $D_{NN'}$ and $S_{NN'}$ for the isotope pair ^{40}Ca and ^{48}Ca in Refs. [2,3]. We reported the data for $P(\theta)$, $A_y(\theta)$, and $(P-A_y)$ for ^{48}Ca in Ref. [4]. In Ref. [5], we compared the $D_{NN'}$ data for self-conjugate targets ^{16}O and ^{40}Ca with distorted-wave impulse-approximation (DWIA) calculations that used Tamm-Dancoff approximation wave functions from Donnelly and Walker [6].

In this paper we present our $S_{NN'}$ data for the ^{208}Pb$(p,n)^{208}$Bi reaction at 0°, 3°, 6°, and 9°, and we compare these data with DWIA calculations that use random-phase approximation (RPA) wave functions. We describe the experimental techniques in Sec. II. We describe briefly the DWIA-RPA formalism in Sec. III. In Sec. IV we compare the data for $S_{NN'}$ for this reaction with the DWIA-RPA calculations; we also present similar comparisons for the ^{48}Ca $(p,n)^{48}$Sc reaction at 0°. We then present the summary and conclusions in Sec. V. Data for $P(\theta)$ and $A_y(\theta)$ are presented in Ref. [7].

II. EXPERIMENTAL TECHNIQUE

We performed this experiment at the Indiana University Cyclotron Facility (IUCF) with the beam-swinger neutron time-of-flight facility. The beam energy was 135.7 MeV. The proton beam current was typically 150 nA, and the beam polarization was typically $+0.65$ and -0.64 for the spin up and spin down beam states, respectively. We measured the beam polarization with $p+^4$He elastic scattering with a polarimeter located between the IUCF injector cyclotron and the IUCF main stage cyclotron. The polarization was reversed every 30 s. The areal density of the ^{208}Pb target was 175.7 ± 3.0 mg cm^{-2}.

The flight path from the target to the neutron polarimeter was 33.7 m. The polarimeter, shown in Fig. 1, is described in detail in Ref. [1]. The polarimeter utilizes the analyzing power of *n-p* elastic scattering from the hydrogen nuclei of the BC-517L mineral oil scintillator in the three scatterers (labeled 1, 2, 3). BC-517L has an H/C atomic ratio of 2.01, and a specific gravity of 0.86. The BC-517L scintillator is contained in acrylic plastic chambers; the active volume of each scatterer is 0.102 m×0.127 m×1.016 m. Scattered neutrons are detected in two sets of ''side detectors,'' labeled 4,5,6 and 7,8,9. The side detectors are made of BC-400 plastic scintillator; each has an active volume of 0.102 m×0.254 m×1.016 m. The central scattering angle in

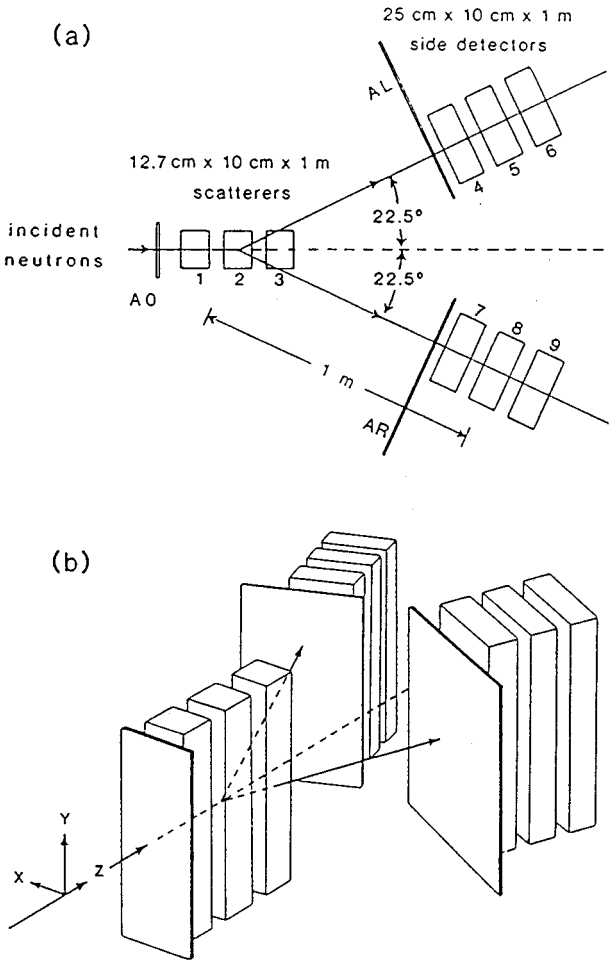

FIG. 1. The configuration of the neutron polarimeter (a) as seen from above and (b) in perspective. A0, AL, and AR are anticoincidence detectors.

the polarimeter is 22.5°, which is near the maximum value of $A_y^2\times\sigma$ for n-p elastic scattering, where A_y is the analyzing power and σ is the laboratory differential cross section. The product $A_y^2\times\sigma$ is the usual ''figure of merit'' for a polarization analyzing reaction. Each of the nine detectors is mean timed with a 126-mm diameter Amperex XP-2041 photomultiplier tube on both the top and bottom ends, coupled to the scintillator with an acrylic plastic light pipe. A0, AL, and AR are anticoincidence detectors to veto charged particles and cosmic rays.

For each event we recorded six parameters: the pulse heights in the scatterer and side counter, the positions of interaction in the scatterer and side counter, the time of flight from the target to the scatterer, and the time of flight between the scatterer and the side counter. In addition, for each event we recorded the identity of the scatterer and side counter involved and the spin state of the beam. From the identity of the scatterer and side detector involved in each event, and the position of interaction in these detectors, we determined (during data replay) Δx, Δy, and Δz for the points of interaction; from Δx, Δy, and Δz we constructed r, θ, and ϕ. The geometry of each event (r, θ, ϕ), and the incident and scattered velocities for each event were used to eliminate most of the events originating from reactions on the carbon

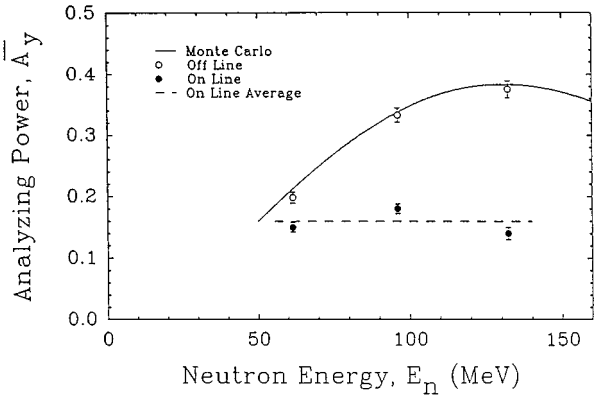

FIG. 2. The analyzing power A_y of the neutron polarimeter as a function of the incident neutron kinetic energy E_n. Shown are on-line results, off-line results for the final software cuts, and results from a Monte Carlo simulation assuming n-p scattering alone.

nuclei in the scatterers; these events, which have a measured analyzing power consistent with zero, are the principal background in the polarimeter. See Ref. [1] for a detailed discussion of the optimization of the software cuts.

We calibrated the analyzing power of the polarimeter with the ^{14}C$(p,n)^{14}$N(2.31 MeV, 0^+) reaction at 0° for beam energies of 65, 100, and 135 MeV. This is a 0^+ to 0^+ transition, and has $D_{NN'}\equiv 1$; therefore, at 0°, where $P=A_y=0$, the neutron polarization $p_n\equiv p_p$, the polarization of the proton. We calibrated the efficiency of the polarimeter by measuring the neutron fluxes from reactions with known cross sections, namely the ^{12}C$(p,n)^{12}$N(g.s., 1^+) reaction [8] and the ^{14}C$(p,n)^{14}$N(3.95 MeV, 1^+) reaction [7,9]. The efficiency is the probability that a neutron passing through the scatterers will produce an event that survives all software cuts.

In Figs. 2 and 3 we present, as a function of neutron energy, the polarimeter analyzing power and efficiency, averaged over the acceptance of the polarimeter, after imposing all software cuts. For the ''on-line'' results, the only cuts were pulse-height thresholds on the scatterers and side detectors. For this experiment, the typical ''off-line'' polarimeter analyzing power was 0.375, and the efficiency was 0.17%.

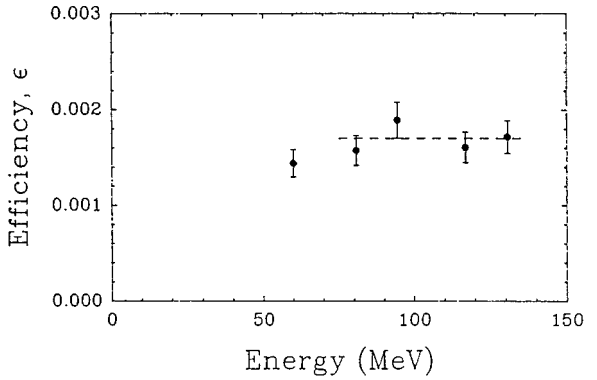

FIG. 3. The efficiency of the polarimeter as a function of the incident neutron kinetic energy E_n. These efficiencies were determined from the ^{12}C$(p,n)^{12}$N(g.s.) and ^{14}C$(p,n)^{14}$N(3.95 MeV) reactions with the final choice of software cuts. The weighted average of the four highest points is 0.17%.

TABLE I. The particle and hole states for the RPA calculations.

Target		
^{208}Pb	Neutron hole states	$1h_{9/2}$, $2f_{7/2}$, $1i_{13/2}$, $2f_{5/2}$, $3p_{3/2}$, $3p_{1/2}$
	Neutron particle states	$2g_{9/2}$, $1i_{11/2}$, $1j_{15/2}$, $3d_{5/2}$, $4s_{1/2}$, $2g_{7/2}$, $3d_{3/2}$
	Proton hole states	$1g_{7/2}$, $2d_{5/2}$, $1h_{11/2}$, $2d_{3/2}$, $3s_{1/2}$
	Proton particle states	$1h_{9/2}$, $2f_{7/2}$, $1i_{13/2}$, $2f_{5/2}$, $3p_{3/2}$, $3p_{1/2}$
^{48}Ca	Neutron holes states	$1s_{1/2}$, $1p_{3/2}$, $1p_{1/2}$, $1d_{5/2}$, $2s_{1/2}$, $1d_{3/2}$, $1f_{7/2}$
	Neutron particle states	$2p_{3/2}$, $1f_{5/2}$, $2p_{1/2}$
	Proton hole states	$1s_{1/2}$, $1p_{3/2}$, $1p_{1/2}$, $1d_{5/2}$, $2s_{1/2}$, $1d_{3/2}$
	Proton particle states	$1f_{7/2}$, $2p_{3/2}$, $1f_{5/2}$, $2p_{1/2}$

The smooth curve in Fig. 2 is the result of a Monte Carlo simulation of the performance of the polarimeter, multiplied by 0.97; this curve was used to obtain the energy dependence of the polarimeter analyzing power. See Ref. [1] for additional details on these calibrations. The ''on-line'' analyzing power of the polarimeter (obtained with pulse-height thresholds as the only ''cuts'') was typically 0.15. This value of the analyzing power was large enough that we could monitor the experiment easily without having to set up an elaborate on-line replay of the data.

The instrumental asymmetry of the polarimeter was determined at 0° where the induced polarization $P(\theta)$ must be identically zero. The measured instrumental asymmetry (a few percent) was then eliminated by adjusting the replay parameters to make $P(\theta)$ zero. The instrumental asymmetry was checked at both the beginning and the end of the run and appeared to have changed but little. The average of the initial and final corrections was used for the analysis of the data for 3°, 6°, and 9°.

The variation of the measured cross section with the angle can, in principle, produce a false asymmetry in the polarimeter for measurements away from 0°. The largest observed cross section variation in this experiment is about 20% per degree. The 0.127 m width of the scatterers in the polarimeter corresponds to about 0.2°, so the maximum variation of the neutron flux across the face of the scatterers is about 4%. From this 4% variation, the geometry of the polarimeter, and the characteristics of *n-p* elastic scattering, we estimate an upper limit to the false asymmetry of 0.5%. With proton beam polarizations of typically 0.65, and a polarimeter analyzing power of 0.375, the maximum true asymmetry we could have observed is about 25%, which would correspond to $D_{NN'}=1.00$. Thus the maximum false asymmetry corresponds to 0.02 in $D_{NN'}$, or 0.01 in $S_{NN'}$; these values are significantly smaller than the statistical accuracy with which we determined $D_{NN'}$ and $S_{NN'}$, and we have ignored any corrections for this possible false asymmetry.

III. DWIA-RPA CALCULATIONS

The DWIA-RPA calculations for both ^{208}Pb and ^{48}Ca are similar to those described by Lisantti *et al.* [10]. Optical potentials were taken from Schwandt *et al.* [11], with the Coulomb term turned off for the exit channel. For the nucleon-nucleon interaction we used the *t* matrix of Franey and Love [12]. To evaluate the importance of distortions for these calculations, we also performed plane-wave impulse-approximation (PWIA-RPA) calculations, where the optical potentials were set equal to zero.

The nuclear structure is described with the 1p-1h RPA with 2p-2h damping in the continuum [13]. We list in Table I the hole and particle basis states for both targets. We used the residual interaction of Rinker and Speth [14], which is a zero-range Landau-Migdal force. We found it necessary to make one modification to this force. To describe correctly the excitation energy of the 0^+ isobaric-analog state (IAS) of the ^{208}Bi and ^{48}Sc residual nuclei, we had to change the f_0' strength parameter (which multiplies the $\tau\cdot\tau$ term) from 1.5 to 0.9. For ^{208}Bi, this moves the IAS from 25 MeV to the correct value of 15.5 MeV, and for ^{48}Sc this moves the IAS from 10 MeV to the correct value of 6.5 MeV. Figures 4 and 5 show the 0° excitation-energy spectrum of 0^+ states predicted for both nuclei with the two different values of f_0'. It is noteworthy that a single change in f_0' produces the correct location of the IAS for both targets. Changing f_0' makes no change in the 1^+ spectrum which describes the Gamow-Teller giant resonance (GTGR); the GTGR dominates the low excitation energy spectrum at small angles.

At 135 MeV there is a non-negligible probability that multistep processes will contribute to the (p,n) continuum.

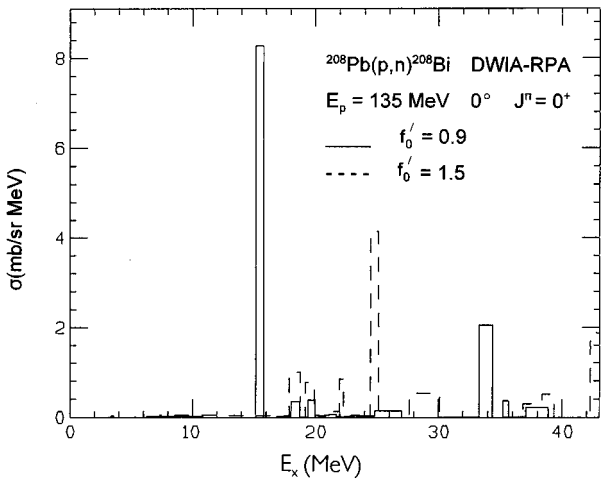

FIG. 4. DWIA-RPA calculations of the spectrum of 0^+ cross section strength at 0° for the ^{208}Pb$(p,n)^{208}$Bi reaction at 135 MeV. The dashed line is the calculation with $f_0'=1.5$; the solid line is the calculation with $f_0'=0.9$. The largest peak is the isobaric-analog state which is located experimentally at 15 MeV.

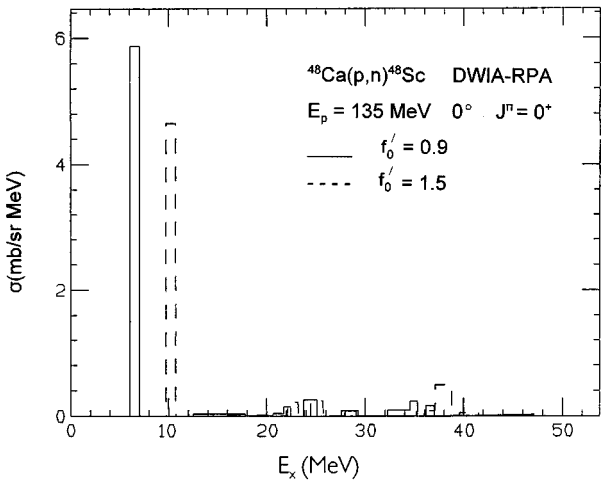

FIG. 5. DWIA-RPA calculations of the spectrum of 0^+ cross section strength at 0° for the ^{48}Ca$(p,n)^{48}$Sc reaction at 135 MeV. The dashed line is the calculation with $f_0'=1.5$; the solid line is the calculation with $f_0'=0.9$. The largest peak is the isobaric-analog state which is located experimentally at 6.67 MeV.

To the cross sections obtained from the single-step DWIA-RPA calculations, we have added multistep (MS) cross sections calculated with the Feshbach-Koonin-Kerman (FKK) method [15].

IV. COMPARISON OF EXPERIMENT AND DWIA-RPA

In Figs. 6, 7, 8, and 9 we present the comparison of our data for the center-of-mass differential cross section and the spin-flip probability $S_{NN'}$ for the ^{208}Pb$(p,n)^{208}$Bi reaction at 0°, 3°, 6°, and 9°, respectively. In Fig. 10 we present the same comparison for the ^{48}Ca$(p,n)^{48}$Sc reaction at 0° using the data originally reported in [2,3]. The data are plotted as a function of the energy loss. For both targets, the small angle, small energy loss ($\omega<25$ MeV for ^{208}Pb, $\omega<20$ MeV for ^{48}Ca) spectra consist primarily of 1^+ excitations, most notably the Gamow-Teller giant resonance (GTGR). For these 1^+ excitations we would expect, in a plane-wave model [16] to find $S_{NN'}\sim\frac{2}{3}$, as is generally the case for our data. The other strong feature of the data is the 0^+ IAS which comes experimentally at $\omega=15.5$ MeV for ^{208}Pb and at $\omega=6.5$ MeV for ^{48}Ca. Since the $0^+\rightarrow0^+$ IAS transition must have $S_{NN'}\equiv0$, we observe a dip in $S_{NN'}$ at the location of the IAS in all spectra.

For comparison with the cross section data (top panel of each figure), we show the MS calculations as a dash-dotted line, the sum of the MS and DWIA-RPA calculations as a solid line, and for reference the sum of the MS and PWIA-RPA calculations as a dashed line. In the comparisons with the ^{208}Pb data, we also show (as a dotted line) the sum of the MS calculation and a DWIA-RPA calculation with a reduction in the strength of the imaginary part of the optical potential by 20% ($W_V\times0.8$), to show the relative insensitivity of these calculations (particularly for $S_{NN'}$) to distortions.

For comparison with the $S_{NN'}$ data (bottom panel of each figure) we show the DWIA-RPA, PWIA-RPA, and (for ^{208}Pb) DWIA-RPA($W_V\times0.8$) calculations, all without inclusion of the MS calculation. The FKK method makes no predictions of spin observables; however, because the calculated MS cross section is a small fraction of the measured cross section for $\omega\leqslant30$ MeV, omitting the MS calculation for $\omega\leqslant30$ MeV makes little difference. For $\omega\geqslant30$ MeV, $S_{NN'}\approx1/2$ for the data and for the PWIA-RPA, DWIA-RPA, and DWIA-RPA($W_V\times0.8$) calculations. $S_{NN'}=1/2$ means that the neutrons are unpolarized. If we assume that in a multistep process the spin direction of the detected particle is randomized, the MS calculation would also correspond to $S_{NN'}=1/2$. Hence neglect of the MS calculation for $\omega\geqslant30$ MeV should not be significant for the comparison with the $S_{NN'}$ data.

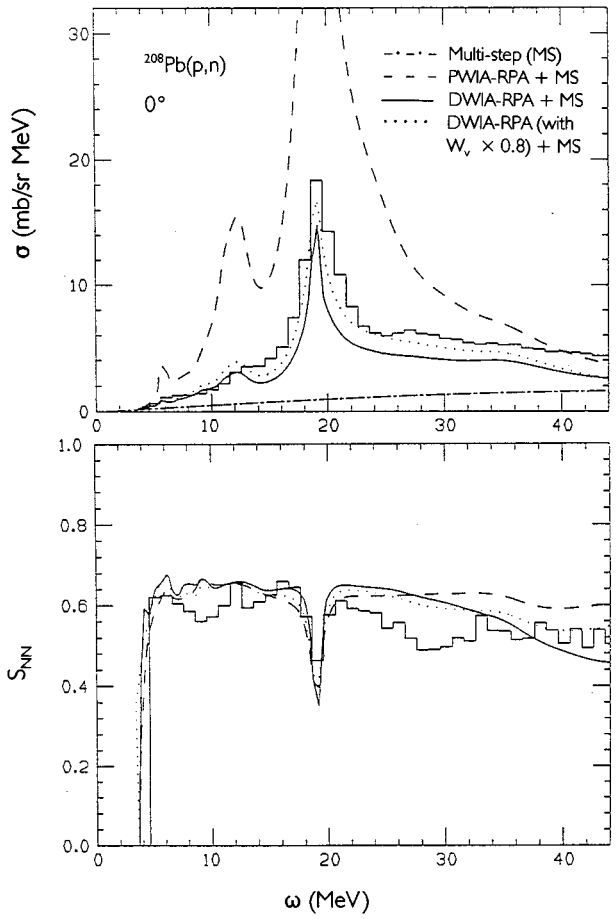

FIG. 6. Data for the differential cross section σ (top panel) and spin-flip probability $S_{NN'}$ (bottom panel) as a function of the energy loss ω for the ^{208}Pb$(p,n)^{208}$Bi reaction at 0°. Shown also are multistep (MS) calculations ($-\cdot-\cdot-\cdot$), DWIA-RPA+MS (——), PWIA-RPA+MS (- - - -), and DWIA-RPA (with $W_V\times0.8$)+MS ($\cdot\cdot\cdot\cdot$). The MS cross section is not included for the $S_{NN'}$ calculations.

For the ^{208}Pb(p,n) reaction, the DWIA-RPA+MS calculations reproduce the general shape of the cross section reasonably well. The calculation with $W_V\times0.8$ reproduces the absolute magnitude of the cross section somewhat better for $\omega\geqslant15$ MeV, but this could be due to underestimation of the MS contribution. For the ^{48}Ca(p,n) reaction the agreement of the DWIA-RPA+MS calculation is significantly worse, due primarily to omission in the RPA of a significant amount of 1^+ strength near $E_x=8$ MeV ($\omega=9$ MeV), seen clearly in

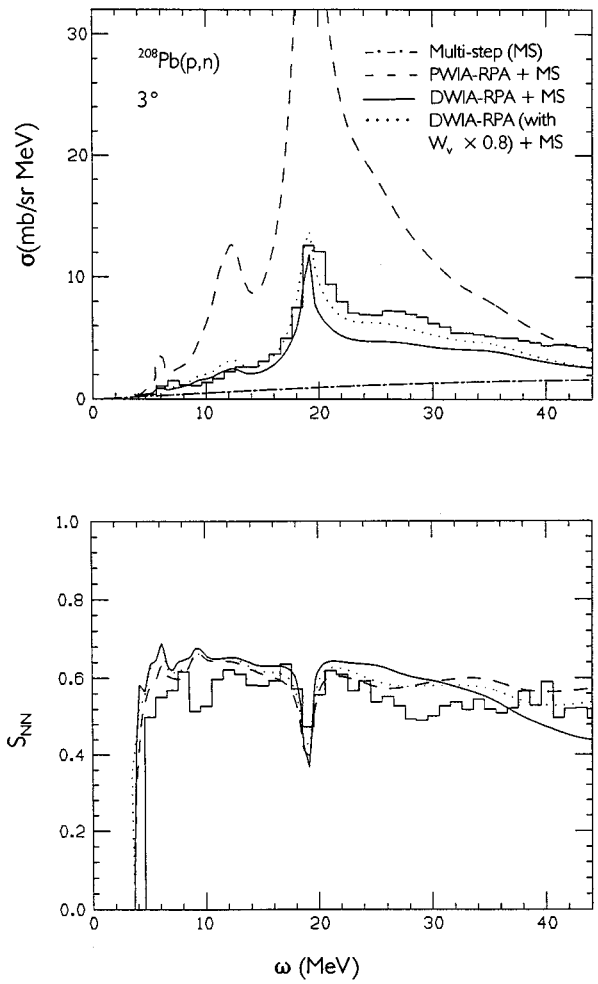

FIG. 7. Data for the differential cross section σ (top panel) and spin-flip probability $S_{NN'}$ (bottom panel) as a function of the energy loss ω for the ^{208}Pb$(p,n)^{208}$Bi reaction at 3°. Shown also are multi-step (MS) calculations ($-\cdot-\cdot-\cdot$), DWIA-RPA+MS (——), PWIA-RPA+MS (- - - -), and DWIA-RPA (with $W_V\times 0.8$)+MS ($\cdot\ \cdot\ \cdot\ \cdot$). The MS cross section is not included for the $S_{NN'}$ calculations.

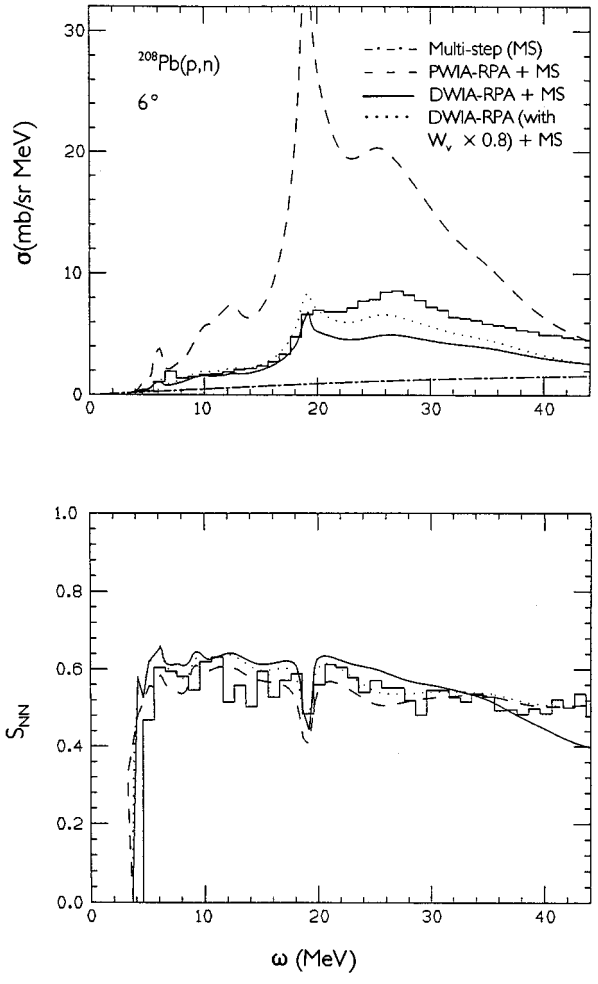

FIG. 8. Data for the differential cross section σ (top panel) and spin-flip probability $S_{NN'}$ (bottom panel) as a function of the energy loss ω for the ^{208}Pb$(p,n)^{208}$Bi reaction at 6°. Shown also are multi-step (MS) calculations ($-\cdot-\cdot-\cdot$), DWIA-RPA+MS (——), PWIA-RPA+MS (- - - -) , and DWIA-RPA (with $W_V\times 0.8$)+MS ($\cdot\ \cdot\ \cdot\ \cdot$). The MS cross section is not included for the $S_{NN'}$ calculations.

the higher resolution 135 MeV cross section data of Anderson *et al.* [8].

For both reactions, all three calculations of $S_{NN'}$ agree generally rather well with the measured values of $S_{NN'}$ except for the region near $\omega=9$ MeV for ^{48}Ca(p,n), for the reasons discussed above. The differences between the three calculations are for the most part small, consistent with the conventional wisdom that ''$S_{NN'}$ is a robust observable.'' The agreement of the DWIA-RPA calculations for ^{208}Pb(p,n) is noteworthy, in light of similar comparisons of $S_{NN'}$ for ^{208}Pb(p,p') at 200 MeV reported in Ref. [10] by Lisantti *et al.* The DWIA-RPA calculations for ^{208}Pb(p,p') reproduced the measured $S_{NN'}$ data quite well, although for that data $S_{NN'}\leqslant 0.25$ over most of its range; by contrast, $S_{NN'}\geqslant 0.40$ for almost all of the (p,n) data for both targets. The (p,p') reaction is mixed isoscalar and isovector, exciting primarily natural parity states, whereas the (p,n) reaction is purely isovector exciting primarily unnatural parity states. As a result, these two reactions have quite different values for $S_{NN'}$, which the DWIA-RPA nevertheless reproduces well.

V. SUMMARY AND CONCLUSIONS

In this paper we reported measurements of the spin-flip probability $S_{NN'}$ for the ^{208}Pb$(p,n)^{208}$Bi reaction at 135 MeV for laboratory angles of 0°, 3°, 6°, and 9°. These data were taken with a high-efficiency neutron polarimeter with a typical polarimeter analyzing power $A_y=0.375$ and an efficiency of 0.17%. For comparison with these data, we performed DWIA-RPA calculations; the RPA calculations are 1p-1h RPA with 2p-2h damping in the continuum. We also performed calculations for the ^{48}Ca$(p,n)^{48}$Sc reaction at 135 MeV for comparison with previously published data. For the RPA calculations, we had to adjust the f_0' parameter in the Landau-Migdal residual interaction to place the 0^+ isobaric analog state (IAS) at the correct excitation energy. A single adjustment of f_0' from 1.5 to 0.9 placed the IAS at the correct energy for both targets.

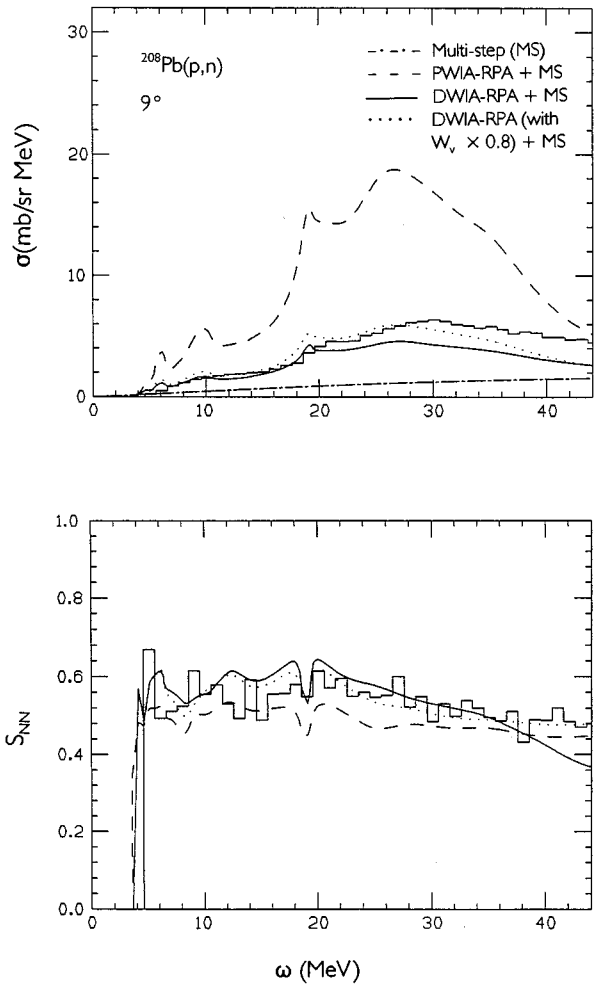

FIG. 9. Data for the differential cross section σ (top panel) and spin-flip probability $S_{NN'}$ (bottom panel) as a function of the energy loss ω for the ^{208}Pb$(p,n)^{208}$Bi reaction at 9°. Shown also are multistep (MS) calculations ($-\cdot-\cdot-\cdot$), DWIA-RPA+MS (——), PWIA-RPA+MS (- - - -), and DWIA-RPA (with $W_V\times 0.8$)+MS ($\cdot\ \cdot\ \cdot\ \cdot$). The MS cross section is not included for the $S_{NN'}$ calculations.

For comparison with the cross section data, we combined the DWIA-RPA cross sections with multistep (MS) cross sections calculated with the Feshbach-Kerman-Koonin method. This combination reproduces fairly well the general trends of the experimental cross sections, except for the ^{48}Ca$(p,n)^{48}$Sc reaction near $\omega=9$ MeV where a significant amount of 1^+ (GT) strength is missed.

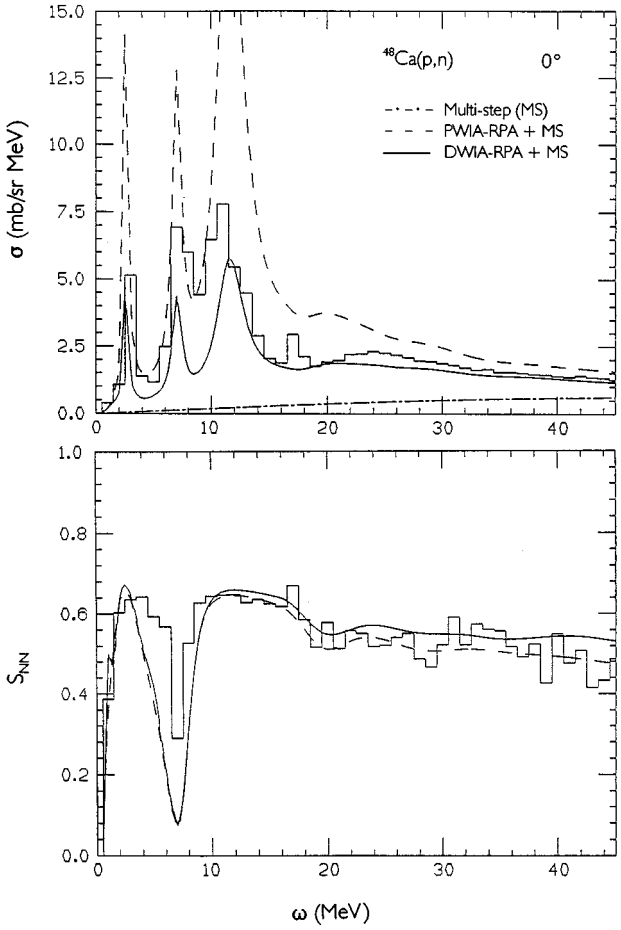

FIG. 10. Data for the differential cross section σ (top panel) and spin-flip probability $S_{NN'}$ (bottom panel) as a function of the energy loss ω for the ^{48}Ca$(p,n)^{48}$SC reaction at 0°. Shown also are multistep (MS) calculations ($-\cdot-\cdot-\cdot$), DWIA-RPA+MS (——), and PWIA-RPA+MS (- - - -). The MS cross section is not included for the $S_{NN'}$ calculations.

The DWIA-RPA calculations for $S_{NN'}$ generally agree well with the data for both targets, except again for ^{48}Ca near $\omega=9$ MeV. PWIA-RPA calculations and DWIA-RPA calculations with the strength of the imaginary part of the optical potential reduced by 20% are very similar to the standard DWIA-RPA calculations, indicating that $S_{NN'}$ is generally insensitive to distortions.

This research was supported in part by the U. S. National Science Foundation.

[1] J. W. Watson, Marco R. Plumley, P. J. Pella, B. D. Anderson, A. R. Baldwin, and R. Madey, Nucl. Instrum. Methods Phys. Res. A **272**, 750 (1988).

[2] J. W. Watson, P. J. Pella, B. D. Anderson, A. R. Baldwin, T. Chittrakarn, B. S. Flanders, R. Madey, C. C. Foster, and I. J. van Heerden, Phys. Lett. B **181**, 47 (1986).

[3] J. W. Watson, B. D. Anderson, and R. Madey, Can. J. Phys. **65**, 566 (1987).

[4] W.-M. Zhang, B. D. Anderson, A. R. Baldwin, T. Eden, D. M. Manley, R. Madey, E. Steinfelds, J. W. Watson, P. J. Pella, and C. C. Foster, Phys. Rev. C **45**, 2819 (1992).

[5] J. W. Watson, B. D. Anderson, A. R. Baldwin, C. C. Foster, D. L. Lamm, R. Madey, P. J. Pella, Y. Wang, and W.-M. Zhang, Nucl. Phys. **A577**, 79c (1994).

[6] T. W. Donnelly and G. E. Walker, Ann. Phys. (N.Y.) **60**, 209 (1970).

[7] Marco R. Plumley, Ph.D. dissertation, Kent State University, 1989.
[8] B. D. Anderson, T. Chittrakarn, A. R. Baldwin, C. Lebo, R. Madey, R. J. McCarthy, J. W. Watson, B. A. Brown, and C. C. Foster, Phys. Rev. C **31**, 1147 (1985).
[9] J. W. Watson, W. Pairsuwan, B. D. Anderson, A. R. Baldwin, B. S. Flanders, R. Madey, R. J. McCarthy, B. A. Brown, B. H. Wildenthal, and C. C. Foster, Phys. Rev. Lett. **55**, 1369 (1985).
[10] J. Lisantti, E. J. Stephenson, A. D. Bacher, P. Li, R. Sawafta, P. Schwandt, S. P. Wells, S. W. Wissink, W. Unkelbach, and J. Wambach, Phys. Rev. C **44**, R1233 (1991).
[11] P. Schwandt, H. O. Meyer, W. W. Jacobs, A. D. Bacher, S. E. Vigdor, M. D. Kaitchuck, and T. R. Donoghue, Phys. Rev. C **26**, 55 (1982).
[12] M. A. Franey and W. G. Love, Phys. Rev. C **31**, 448 (1985).
[13] Richard D. Smith, *Spin Observables of Nuclear Probes* (Plenum, New York, 1988), p. 15; R. D. Smith and J. Wambach, Phys. Rev. C **38**, 100 (1988).
[14] G. A. Rinker and J. Speth, Nucl. Phys. **A306**, 360 (1978).
[15] H. Feshbach, A. Kerman, and S. Koonin, Ann. Phys. (N.Y.) **125**, 420 (1980).
[16] W. D. Cornelius, J. M. Moss, and T. Yamaya, Phys. Rev. C **23**, 1364 (1980).